Physics of Plasmas ARTICLE scitation.org/journal/php

# Gyrokinetic and extended-MHD simulations of a flow shear stabilized Z-pinch experiment

Cite as: Phys. Plasmas **28**, 052113 (2021); doi: 10.1063/5.0037506
Submitted: 16 November 2020 · Accepted: 20 April 2021 ·
Published Online: 26 May 2021



V. I. Geyko,[a] J. R. Angus, and M. A. Dorf

## AFFILIATIONS

Lawrence Livermore National Laboratory, Livermore, California 94550, USA

[a]Author to whom correspondence should be addressed: geyko1@llnl.gov

## ABSTRACT

Axisymmetric ($m = 0$) gyrokinetic and extended-MHD simulations of a sheared-flow Z-pinch plasma are performed with the high-order finite volume code COGENT. The present gyrokinetic model solves the long-wavelength limit of the gyrokinetic equation for both ion and electron species coupled to the electrostatic gyro-Poisson equation for the electrostatic potential. The extended-MHD model is electromagnetic and includes the effects of the gyro-viscous pressure tensor, diamagnetic electron and ion heat fluxes, and generalized Ohm's law. A prominent feature of this work is that the radial profiles for the plasma density and temperature are taken from the fusion Z-pinch experiment (FuZE), and the magnetic field profile is obtained as a solution of the MHD force balance equation. Such an approach allows to address realistic plasma parameters and provide insights into the current and planned experiments. In particular, it is demonstrated that the radial profiles play an important role in stabilization, as the embedded guiding center ($E \times B$) drift has a strong radial shear, which can contribute to the Z-pinch stabilization even in the absence of the fluid flow shear. The results of simulations for the FuZE plasma parameters show a decrease in the linear growth rate with an increase in the flow shear; however, full stabilization in the linear regime is not observed even for large (comparable to the Alfvén velocity) radial variations of the axial flow. Nonlinear stability properties of the FuZE plasmas are also studied, and it is found that profile broadening can have a pronounced stabilizing effect in the nonlinear regime.



## I. INTRODUCTION

From the dawn of magnetic fusion energy studies, the Z-pinch concept has been considered as a possible plasma confinement configuration suitable for maintaining a controlled fusion reaction.[1,2] The Z-pinch configuration is a cylindrically symmetric plasma column with an axial current inside, such that the generated magnetic field creates an inward Lorentz force that confines the plasma. Relatively simple cylindrical geometry and the absence of any external magnetic fields together with a great utilization of the generated magnetic field ($\beta \sim 1$) make this concept quite attractive. However, Z-pinch plasmas are susceptible to rapid magnetohydrodynamics (MHD) instabilities, whose growth rate $\gamma_i$ is on the order of the inversed Alfvén time $\gamma_i \sim V_a/a$, where $V_a$ is the Alfvén speed and $a$ is the characteristic radial size of the pinch. The instabilities completely disrupt the pinch as was observed in certain experiments.[2–4] The local linear MHD analysis of these instabilities was done by Kadomtsev,[5] and it was shown that the most unstable modes are $m = 0$ and $m = 1$, called *sausage* and *kink* modes, respectively, where $m$ is the angular number. Apart from MHD modes, which typically have a spatial scale of the pinch radius, short-wavelength drift modes with scale on the order of ion gyroradius $\rho_i$ and growth rate on the order[6,7] $\gamma_d \sim (k_\perp \rho_i) V_a/a$ can develop as well. Here, $k_\perp$ is the wave vector in the perpendicular to the magnetic field direction. These modes appear naturally in gyrokinetic formulation[6,8] and can also be captured with extended-MHD models[5,9] if proper drift terms are retained. For the wavelengths on the order of the ion gyroradius, these modes can be as destructive as the ideal MHD modes; therefore, the problem of Z-pinch stabilization becomes even more complicated.

A renewed interest to the concept was prompted by the recent successful experiments on the sheared flow stabilized (SFS) Z-pinches, namely, ZaP[10–12] and fusion Z-pinch experiment (FuZE).[13–15] The most recent FuZE experiment reports a pinch with a current of 200 kA stable for approximately 5000 Alfvén times, which is drastically greater than characteristic linear instability growth time. In both experiments, an axially sheared plasma flow is believed to play a key stabilizing role. While there are no reported values of shear for the FuZE, the ones from the ZaP experiment are somewhat a fraction of the Alfvén velocity over the pinch radius[16,17] $a$.

The idea of using a sheared flow for stabilization of Z-pinch plasmas originates from early work of Shumlak and Hartman,[18] where

they demonstrated that a moderate shear is capable of stabilizing the $m=1$ MHD mode, provided $dv_z/dr \geq 0.1kV_a$, where $k$ is the axial wave vector and $v_z$ is the plasma flow velocity. This result was obtained for the Kadomtsev profile,[5] which is marginally stable against the $m=0$ MHD mode. However, these results are in disagreement with Arber's work[19] where no pronounced mitigation of the $m=1$ mode with the wavelength $ka=10/3$ was observed even for larger values of flow shear. A more detailed recent study[20] on the stability of linear ideal MHD modes did not support the original hypotheses either. Nonlinear ideal-MHD simulations of the $m=0$ mode were done by Paraschev,[21] and a different stabilization condition was reported $dv_z/dr \geq V_a/a$. The ideal MHD model is, however, of limited validity because of relevant experimental parameters for which (i) the plasma is hot and therefore not strongly collisional, (ii) the ion Larmor radius is not infinitesimally small, $\rho_i/a \sim 0.1$, and therefore, finite Larmor radius (FLR) effects have to be taken into account. To overcome these issues, extended-MHD,[9] gyrokinetic,[22] and fully kinetic[23] simulations were performed by different authors. The main difference between the kinetic and ideal-MHD models is that the linear growth rate can decrease for $k\rho_i \gtrsim 1$ due to FLR effects,[24] which is not observed in the ideal MHD simulations. The stabilizing effect by a sheared flow on the $m=0$ mode was observed in all the simulations, yet, no complete stabilization by the moderate shear was demonstrated in the gyrokinetic simulations.[22] Furthermore, the stabilization of the $ka=5.0$ mode only was reported in the fully kinetic simulations,[23] and no data for other wavelengths were obtained.

The aforementioned simulations were performed for the case of some special model profiles for density and temperature. The most common choice was the diffuse Bennett[25,26] profile, which has a unique property of being an equilibrium solution for a fully kinetic formulation. A noticeable feature of this profile is that it has a moderate logarithmic derivative of the pressure, and depending on the adiabatic gas index $\Gamma$ the profile is either stable or unstable at all $r$ for the $m=0$ mode.[9] A *realistic* profile obtained from recent experimental data[13] is, however, drastically different from the Bennett model profile. Therefore, the stability properties of the FuZE plasmas can be substantially different from those obtained in the previous numerical studies.

In the present paper, we make use of the COGENT[27] code to simulate the $m=0$ mode behavior in a realistic (also called *FuZE-like*) type of pinch profiles. The simulations are performed by making use of the electrostatic and extended-MHD simulation models. The gyrokinetic formulation employs the electrostatic full-F long-wavelength approximation. This model was tested and compared[22] to fully kinetic Particle-in-Cell (PIC) simulations, and it was shown to adequately capture physics related to FLR effects. The model is missing electromagnetic effects and higher order FLR effects, as well as the capability to deal with thermal-range flow velocities. The extended-MHD model includes a gyroviscous pressure tensor based on Braginskii formulation, generalized Ohm's law and diamagnetic electron and ion heat fluxes in the energy density equations. As mentioned earlier, the MHD model has a limited validity for the parameters characteristic to the FuZE plasmas. Nevertheless, its formulation consistently include electromagnetic effects and allows for arbitrary large shear values. While a better extension of the model is needed in order to correctly capture collisionless ion FLR physics (for example, a Chew–Goldberger–Low model can be considered[28]), the results can still provide good insights on the plasma behavior and shear flow stabilization process. Both models demonstrate that a moderately sheared flow is not sufficient to provide a global pinch stabilization. In addition, the effects of a profile shape on the stability properties have been addressed, and it is found that profile broadening can have a pronounced stabilizing effect in the nonlinear regime.

The paper is organized as follows. Section II contains theoretical background including data fitting, scaling analysis, and a review on the main results obtained in the previous work. Details and results of the gyrokinetic simulations are shown in Sec. III. The MHD model equations and simulations are covered in Sec. IV. Speculations on possible stabilization mechanism for broad pinch profiles are provided in Sec. V. In Sec. VI, the main results are summarized.

## II. THEORETICAL BACKGROUND

### A. Realistic profiles

We define a set of functions that describe the radial dependence of the plasma density $n(r)$ and temperature $T(r)$ as a "FuZE-like profile" if these functions are obtained via a nonlinear curve fitting of the FuZE experimental data. The data are provided in the recent work of Zhang *et al.*[13] In particular, the density and temperature data are shown in Figs. 3(b) and 4(b) of the cited work, respectively. The data are fitted with smooth analytical functions in order to be used as the initial conditions for numerical simulations.

While there are two profiles for density provided in Ref. 13, measured at axial locations of $z=13.8$ cm and $z=15.0$ cm, only the former is used in the present work. The most noticeable difference between them is observed at the interior of the pinch close to the axis, yet the simulated mode of interest is localized close to the periphery, thus making this difference negligible. Moreover, the data at $r=0$ are very noisy and irregular, so that it cannot be fitted well. Therefore, using both profiles is unnecessary and the only one is picked for all the simulations here.

There is an infinite amount of possible fitting functions, yet, they have to satisfy the following constraints in order to obtain a reasonable setup. First, the radial derivative of the total pressure at $r=0$ should be zero; otherwise, the curl of the magnetic field has an irregular point, hence a divergent current density on the axis of the pinch (see Sec. II B for more details). Second, since the simulated instabilities are localized on the periphery,[22] the match between the fitting function and the data on the periphery is more important than in the interior of the pinch. Third, the experimental data are provided in the interval $r \in [0; 0.5]$ cm, which does not define the extension of the fitting function at $r>0$. The main driver of the linear mode[5,9] (the radial logarithmic derivative of the pressure $\frac{r}{P}\frac{dP}{dr}$) and, as a result, the stability and spatial location of the mode are fully determined by the choice of the fitting function. The driver can be made arbitrary large by making the density small; therefore, the fitting function should be chosen such that the spatial location of the mode overlaps with the experimental data considerably. This can be achieved by an addition of some small floor to the density function.

Taking into account all the requirements, the following fitting function is introduced:

$$\frac{n(r)}{n_0} = 0.05 + 0.855 \cdot \exp\left(-\frac{r^2}{0.32} - \frac{r^4}{0.0177}\right), \tag{1}$$

where $n_0 = 10^{17}\,\mathrm{cm}^{-3}$, and the radius $r$ is measured in centimeters. Notice that the density has a floor value 0.05. As it was mentioned, it

helps to confine the spatial perturbation of the linear mode at some reasonable radial location. The experimental data with the applied fitting are shown in Fig. 1.

The data for temperature are much more irregular and cannot be fitted well by any smooth function. In this particular realization, the following fitting is used:

$$\frac{T(r)}{T_0} = 0.4015 + 1.0893 \cdot \exp\left[-8.0148(r + 0.26)^2\right], \quad (2)$$

where $T_0 = 1.0$ keV, and the radius is again in centimeters. The measured data are centered at $\tilde{r}_0 = -0.26$ cm, because the pinch in the experiment moved as a whole from the initial axis when the measurements were performed. This effect is ignored in the present research and the pinch is assumed to be always centered. Thus, the adjusted radial temperature profile reads as

$$\frac{T(r)}{T_0} = 0.4015 + 1.0893 \cdot \exp\left[-8.0148r^2\right] \quad (3)$$

and is illustrated in Fig. 2 together with the experimental data.

The self-consistent magnetic field of the equilibrium can be found from the force balance equation $\nabla P = \mathbf{J} \times \mathbf{B}$, or

$$\frac{\partial P}{\partial r} + \frac{1}{8\pi}\frac{\partial (B^2)}{\partial r} + \frac{B^2}{4\pi r} = 0. \quad (4)$$

Here, pressure $P(r) = P_i + P_e = [n_i(r) + n_e(r)]T(r)$ is the total plasma pressure, and $B$ is the magnetic field. The solution of Eq. (4) is

$$\frac{B^2}{4\pi} = \frac{b_0}{r^2} - \frac{2}{r^2}\int_0^r \tilde{r}^2 \frac{\partial P}{\partial \tilde{r}} d\tilde{r}, \quad (5)$$

where $b_0/r^2$ is the "vacuum" term, i.e., the vacuum magnetic field generated by a $\delta$-function current at $r = 0$, which is absent in the current setup. The second term is of interest, as it describes the magnetic field generated by plasma current. For some analytical profiles (for example,

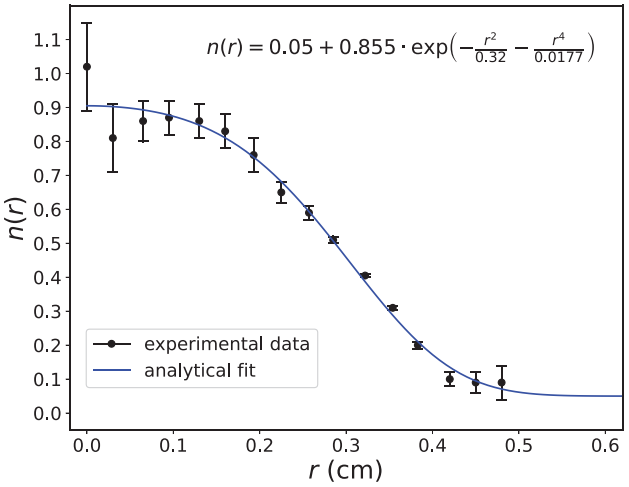


**FIG. 1.** Least squares density fitting with a smooth function. Data points and error bars are taken from the experimental results.[13] All points are taken with the same weights.

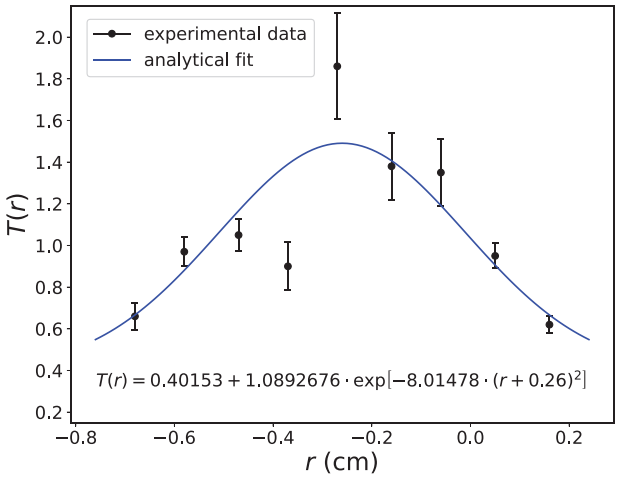


**FIG. 2.** Least squares temperature fitting with a smooth function. Data points and error bars are taken from the experimental results.[13] All points are taken with the same weights.

Bennett), the integral in Eq. (5) can be computed exactly. It follows from Eq. (4) that $\partial P/\partial r$ should be equal to zero at $r = 0$, because otherwise the integrated result scales as $r^3$ for small $r$, thus the magnetic field goes as $B \propto \sqrt{r}$, which is an unphysical behavior, as the corresponding current density is divergent at $r = 0$. This requirement imposes constraints on fitting profiles, as not any arbitrary smooth profile yields a smooth magnetic field profile. The profiles used for density in Eq. (1) and temperature in Eq. (2) satisfy this constraint.

It is convenient to write Eq. (5) in a dimensionless form where the following variable normalization is used: $B = B_0\bar{B}$, $n = n_0\bar{n}$, $T = T_0\bar{T}$, $P = n_0T_0\bar{P}$, where $n_0$ and $T_0$ were introduced earlier, $B_0^2 = 4\pi n_0 T_0$, and $\xi = r/a$. Notice that in such a normalization, characteristic ion thermal and Alfvén velocities are equal $V_{ti}^2 = T_0/m_i = V_a^2 = B_0^2/(4\pi n_0 m_i)$. This fact is widely used throughout the present paper, as all the velocities are normalized to either thermal or Alfvén velocity, which is the same. The solution Eq. (5) reads as

$$\bar{B} = \sqrt{\frac{-2}{\xi^2}\int_0^\xi \tilde{\xi}^2 \frac{\partial \bar{P}}{\partial \tilde{\xi}} d\tilde{\xi}}. \quad (6)$$

The integral in Eq. (6) can be computed numerically for any set of points $\xi_i$. Similarly to the Bennett profile, the characteristic radial size of the FuZE-like profile is defined at the position of the maximum magnetic field, in particular, in our case it is $a = 0.37$ cm. Figure 3 shows the comparison between Bennett and FuZE-like profiles. The latter has much sharper features of the pressure and magnetic field, hence higher logarithmic pressure gradients and greater anticipated linear growth rates.

## B. Fluid and mass flow

A charged particle in a strong magnetic field moves freely with $v_\parallel$ along the field direction $\mathbf{b}$ and orbits around the guiding center with the perpendicular velocity $v_\perp$. The guiding center drifts in the

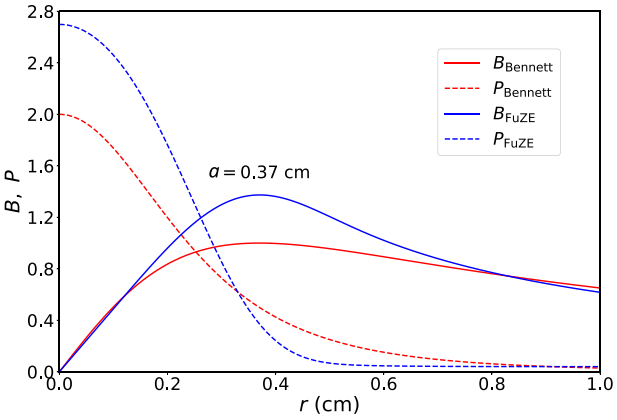


**FIG. 3.** Comparison of the Bennett and FuZE-like profiles for the same value of the normalization $n_0$ and $T_0$. Both profiles have the maximum value of the magnetic field at $a = 0.37$ cm.

perpendicular direction[29] with $\dot{\mathbf{R}}$, so that the guiding center velocity and the parallel acceleration are given by

$$\dot{\mathbf{R}}_\alpha = v_\parallel \mathbf{b} + c\frac{m_\alpha v_\parallel^2}{q_\alpha B}(\nabla \times \mathbf{b})_\perp + \frac{c}{q_\alpha B}\mathbf{b} \times (q_\alpha \nabla\phi + \mu_\alpha \nabla B), \quad (7)$$

$$\dot{v}_{\parallel\alpha} = -\left[\frac{\mathbf{b}}{m_\alpha} + \frac{cv_\parallel}{q_\alpha B}(\nabla \times \mathbf{b})_\perp\right] \cdot (q_\alpha \nabla\phi + \mu_\alpha \nabla B). \quad (8)$$

Here, $\alpha$ denotes the species of the particles, ions, and electrons in this case, $m_\alpha$ and $q_\alpha$ are the particle mass and charge, $c$ is the speed of light, $\mu = m_\alpha v_\perp^2/(2B)$ is the particle magnetic moment, and $\phi$ is the electrostatic potential. In the axisymmetric cylindrical geometry, Eq. (7) simplifies, and the axial component of the guiding center drift velocity reads as

$$\dot{R}_{\alpha,z} = c\frac{m_\alpha v_\parallel^2}{q_\alpha r B} + \frac{c}{q_\alpha B}\left(q_\alpha E_r - \mu\frac{\partial B}{\partial r}\right). \quad (9)$$

Assuming a Maxwellian distribution function and making use of Eq. (9), the axial component of the mean drift velocity can be found,

$$V_{gc,\alpha} = \frac{1}{n_\alpha}\int_{v^3} \dot{R}_{\alpha,z} f_\alpha(\mathbf{x},\mathbf{v}) d^3v = \frac{c}{B}\left[E_r + \frac{T}{q_\alpha r}\left(1 - \frac{r}{B}\frac{\partial B}{\partial r}\right)\right], \quad (10)$$

where $E_r = -\frac{\partial\phi}{\partial r}$ is the radial component of the electric field. The first term in the right-hand side of Eq. (10) is the $E \times B$ drift, and the last term is the combination of magnetic drifts. For a given pressure and plasma flow profiles, the electric field is uniquely defined[29] from the following equation:

$$\frac{\mathbf{v}_{i,e}}{c} = \frac{\mathbf{E} \times \mathbf{B}}{B^2} \mp \frac{\nabla P_{i,e} \times \mathbf{B}}{q n_{i,e} B^2}, \quad (11)$$

where $q$ is the elementary charge, and singly ionized ions $q_i = -q_e = q$ are considered for simplicity. Equation (11) is the expression for the fluid velocities of ions and electrons $\mathbf{v}_{i,e}$ in terms of the $E \times B$ and diamagnetic drifts. For stationary ions $\mathbf{v}_i = 0$, the difference between the $E \times B$ and total drift velocity of ions and electrons Eq. (10) is illustrated in Fig. 4, where the parameters are those from the FuZE-like pinch.

For an axisymmetric cylindrical geometry, Eq. (11) simplifies to

$$\frac{\hat{z} \cdot \mathbf{v}_{i,e}}{c} = \frac{E_r}{B} \mp \frac{\partial P_{i,e}}{\partial r}\frac{1}{q n_{i,e} B}. \quad (12)$$

For subthermal flows, ion fluid velocity $v_{zi}$ is a fraction of the thermal velocity $V_{ti} = \sqrt{T_i/m_i}$, thus the first term in Eq. (12) scales as $V_{ti}/c$. The second term on the right-hand side of Eq. (12) scales as

$$\frac{\partial P_{i,e}}{\partial r}\frac{1}{q n_{i,e} B} \propto \frac{nT}{aqnB} \propto \frac{V_{ti}}{c}\frac{V_{ti}}{\omega_{ci} a} \propto \epsilon\frac{V_{ti}}{c}, \quad (13)$$

where $a$ is the characteristic radial scale of the pinch, $\omega_{ci} = qB/(m_i c)$ is the ion cyclotron frequency and the magnetization parameter $\epsilon = \rho_i/a = V_{ti}/(a\omega_{ci})$. In strongly magnetized plasmas, $\epsilon \ll 1$; thus, the fluid velocity is approximately equal to the drift velocity. Therefore, a fluid shear flow is required for the existence of the $E \times B$ velocity shear and vice versa. This assumption is violated in the case of FuZE-like profiles. First, the parameter $\epsilon$ is not vanishingly small, but instead is equal to $0.1 - 0.2$ depending at what location inside the pinch it is measured. Second, the profile itself has very sharp gradients, so the last term in Eq. (12) becomes comparable to the other terms, therefore strong $E \times B$ velocity shear can be present even in the absence of the fluid flow. In this work, we consider linear shear flow, $V_{sh} = \kappa V_a r/a$, and the parameter $\kappa$ is called a *shear parameter*. Figure 5 demonstrates how the $E \times B$ velocity depends on the radius for the FuZE-like profile for 5 different values $\kappa$. Figure 6 shows the radial derivative of the $E \times B$ velocity for the same values of $\kappa$. There is a very noticeable spike of the derivative at $r/a \approx 1.3$, where embedded shear value corresponds to $\kappa \approx 1.5$.

The conjecture is made here, that in collisionless plasmas, the instability dynamics is predominantly determined by the guiding center velocity, as the motion of every individual particle is only determined by drifts. As it follows from Fig. 4, the difference between the

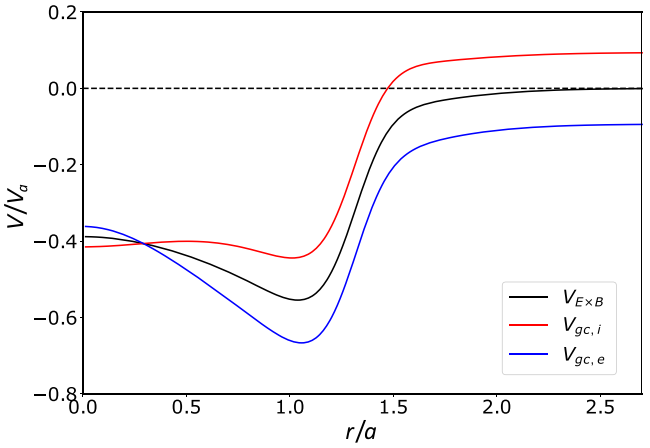


**FIG. 4.** Axial components of the normalized drift velocities for FuZE-like pinch equilibrium: $E \times B$ drift compared to the total ion and electron drifts. All velocities are normalized to the Alfvén velocity $V_a$.

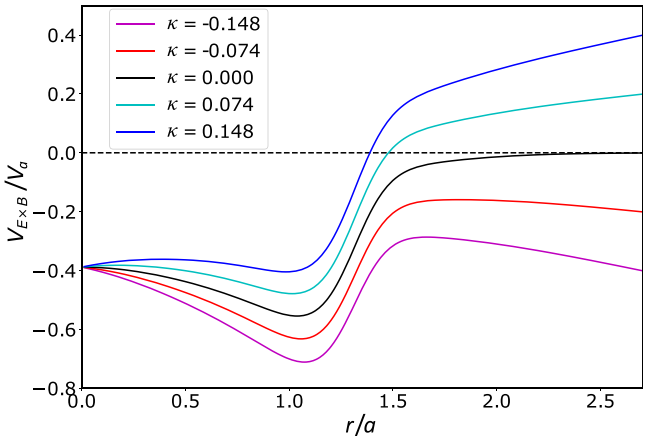


**FIG. 5.** Normalized $E \times B$ velocity as a function of radius for different values of shear parameter $\kappa$.

guiding center velocity and the $E \times B$ velocity is small, especially, when the radial derivative is considered. Assuming the conjecture is true, the two conclusions follow. First, if there is an embedded shear of the drift motion in the system, the amount of the fluid flow shear required to change the system behavior should be at least comparable to the intrinsic value of the guiding center shear. Second, if any stabilization via sheared flow exists, then it should apply to the embedded guiding center velocity shear as well, therefore addition of an extra fluid flow shear can be both stabilizing or destabilizing, depending on how the fluid shear is related to the embedded one. For example, for the FuZE-like profile, positive $\kappa$ increases the radial derivative of the $E \times B$ velocity, while negative $\kappa$ decreases (see Fig. 6); hence, more suppression of the linear mode should be anticipated for positive $\kappa$.

Returning to the comparison of different pinch profiles, notice a peculiarity of the commonly used Bennett profile. The diamagnetic term in Eq. (13) is independent of $r$ for any values of the parameter $\epsilon$, which means that the Bennett profile is unique, as no embedded shear of the $E \times B$ drift is present. Moreover, even the total guiding center

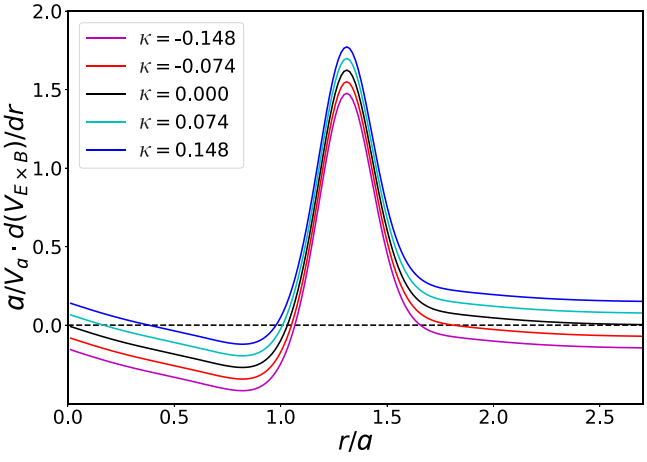


**FIG. 6.** Radial derivative of the normalized $E \times B$ velocity as a function of radius for different values of shear parameter $\kappa$.

drift, including the magnetic field corrections in Eq. (10), does not depend on $r$ either. As a consequence of that, simulations based on the Bennett profile do not provide a general picture, as they are lacking important physics related to the embedded guiding center drift shear.

## III. GYROKINETIC SIMULATIONS

The gyrokinetic simulations are performed with the high-order finite volume code COGENT.[27] The code numerically solves the following equation for the gyro-distribution function $f_\alpha$,

$$\frac{\partial}{\partial t}\left(B^*_{\parallel\alpha} f_\alpha\right) + \nabla_{\mathbf{R}} \cdot \left(\dot{\mathbf{R}}_\alpha B^*_{\parallel\alpha} f_\alpha\right) + \frac{\partial}{\partial v_\parallel}\left(\dot{v}_{\parallel\alpha} B^*_{\parallel\alpha} f_\alpha\right) = 0, \tag{14}$$

where $\nabla_{\mathbf{R}}$ denotes a differential operator with respect to the guiding center coordinates, $\mathbf{b} = \mathbf{B}/B$ is the unit vector in the direction of the magnetic field, $B_{\parallel\alpha} = \mathbf{B}_{\parallel\alpha} \cdot \mathbf{b}$, and

$$\mathbf{B}_{\parallel\alpha} = \mathbf{B} + \frac{m_\alpha c v_\parallel}{q_\alpha} \nabla \times \mathbf{b}. \tag{15}$$

The guiding center drift and parallel acceleration are given by Eqs. (7) and (8), respectively. The simulations are performed in the 2D cylindrical configuration space $(r, z)$ with angular symmetry assumed, and the 2D velocity space $(v_\parallel, \mu)$. The simulation domain has radial boundaries at $r = 0.18$ and $r = 0.82$ cm, with 64 cells in the radial direction and 32 cells in the axial direction. The domain and the density fitting function floor in Eq. (1) are chosen such that the spatial mode is localized away from the external radial boundary at $r = R_{\max}$ in order to eliminate any possible boundary stabilization effects. In the axial direction, only one full wavelength of the mode is seeded. The domain spans from $z = 0$ to $z = \lambda$, where different values of $\lambda$ are tested (from 0.16 to 2.56 cm). Periodic boundary condition is applied in the axial direction. Dirichlet boundary condition at $r = R_{\max}$ and Neumann at $r = R_{\min}$ are used for the potential. The linear growth rate is measured as a function of the wave vector $k_z = 2\pi/\lambda$ for different values of $\kappa$. More details of the simulations and the methodology of the measurements are provided in the previous work of Geyko *et al.*[22]

Linear growth rates obtained from the simulations are shown in Fig. 7, and the main observations are the following. First, the growth rate curve $\gamma(k_z)$ has the same shape as the one obtained for the Bennett case,[22] namely, it has a roll-over at high $k_z$ part of the spectra. Second, the main difference now is that the problem has become shear direction dependent, and a moderate fluid shear ($\kappa \sim 0.2$) can play even a destabilizing role, if the direction is not properly chosen. Finally, the growth rate dependence on $\kappa$ is quite weak, and no stabilization is observed for $\kappa$ on the order of a fraction of unity.

All these observations are in agreement with the conjecture in Sec. II B. Indeed, if the guiding center shear is what determines linear mode stability, then slightly changed by the fluid flow shear (according to Fig. 6), it does not have a significant effect on the growth rate. If stronger shear is required for better stability, then according to Fig. 6 positive fluid flow shear $\kappa > 0$ should lead to more mode stabilization and negative shear $\kappa < 0$ should do the opposite, exactly what is demonstrated in Fig. 7. It also follows from the conjecture that for the fluid flow shear to be comparable to the intrinsic $E \times B$ velocity shear, it should be at least $\kappa \approx 1.5$, i.e., superthermal (or super-Alfvénic) shear, which is not observed in the experiments.

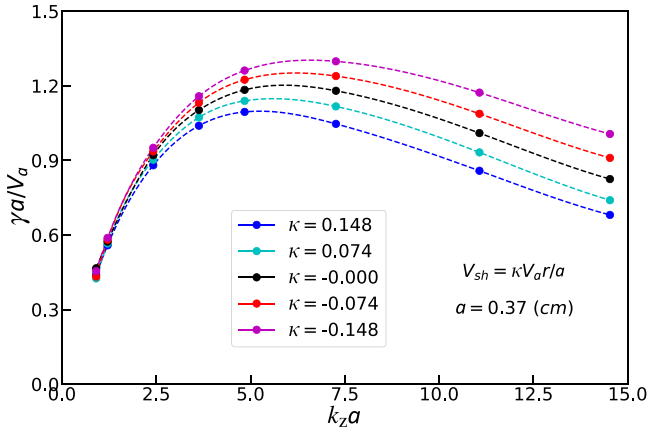


**FIG. 7.** Normalized growth rate of the linear $m = 0$ mode for the FuZE-like profile as a function of the axial wave vector $k_z a$. Five different values of the shear parameter are considered.

As no linear mode mitigation is revealed in the numerical simulations, the source of Z-pinch stabilization in the experiments remains unclear. To address this question, we look at the nonlinear evolution of the system simulated for different values of the domain size in the axial direction, namely, $\lambda = 0.32$ and $\lambda = 0.96$ cm. In both cases, linear modes with the corresponding wavelengths are initially seeded and evolve to the nonlinear stage. Strictly speaking, a nonlinear evolution assumes presence of all the modes supported by the system; therefore, artificial limitation on the domain size cuts off the long-wavelength part of the spectra and does not provide a complete physical picture. The case of the small domain ($\lambda = 0.32$) is nevertheless studied both for academic purposes and also for comparison with the similar evolution of the turbulence in the Bennett profile case. Figures 8 and 9 show the density plots of the nonlinear evolution for $\lambda = 0.32$ and $\lambda = 0.96$ cm modes, respectively. The main difference is that the perturbations of the short-wavelength mode are located on the periphery and do not propagate into the interior of the pinch. The bulk of the pinch is then not perturbed, and therefore, a nonlinear stability can be claimed. In order to verify this conjecture, the evolution of the initial perturbation is diligently monitored throughout entire evolution. The maximum amplitude of the perturbations and disturbance of the pinch occur at the time of transition from linear to nonlinear stages [$t \approx 11.6\, a/V_a$, see Fig. 8(a)], yet the perturbation is not sufficient to completely disturb the pinch. Figure 8(b) shows late time nonlinear evolution, where perturbations have smaller amplitude and are well-localized on the periphery of the pinch. It is not the case for the long-wavelength modes though, as illustrated in Fig. 9. The perturbations reach the inner boundary of the simulation domain, and, in principle, they can possibly spread into the interior of the pinch.

It is interesting to compare the nonlinear evolution of the same wavelength for Bennett and FuZE-like profiles, in particular, a case of nonlinear stabilization of the FuZE-like pinch. Two similar normalized wavelengths are chosen: $k_z a = 7.26$ for FuZE-like and $k_z a = 7.5$ for Bennett cases. Figure 10 demonstrates that nonlinear perturbations of the mode for the Bennett pinch are not confined on the periphery and

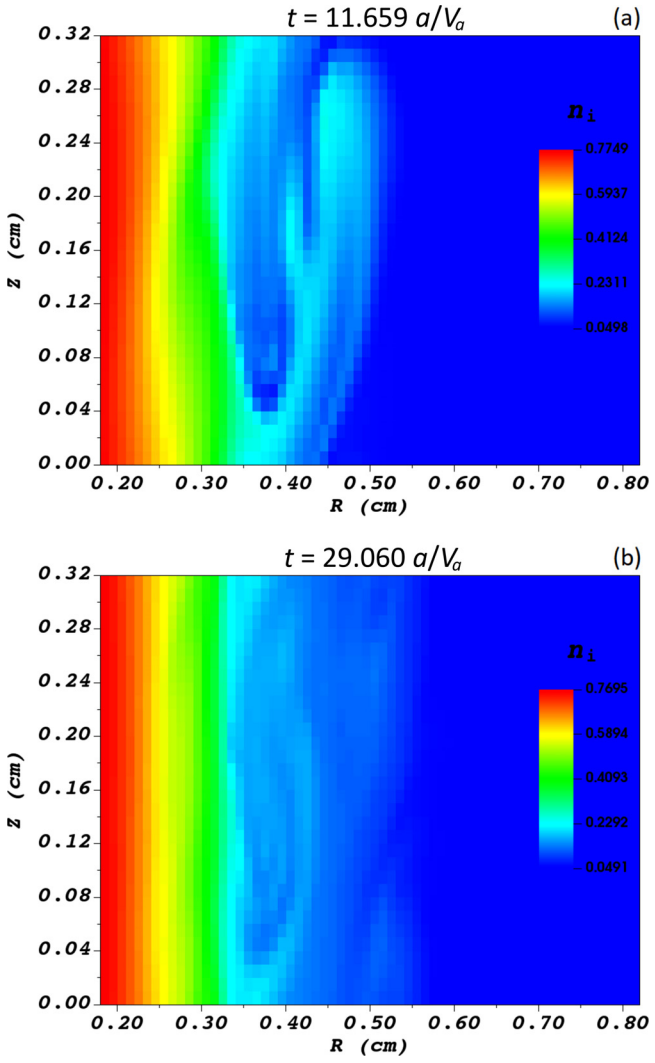


**FIG. 8.** Gyrokinetic simulations of the $m = 0$, $k_z a = 7.26$ mode for the FuZE-like profile. Plots demonstrate normalized ion gyrokinetic density distribution. Plot (a) shows the transition from the linear to nonlinear stages, where the amplitude of the perturbations is at maximum. Plot (b) shows the nonlinear evolution at later time, where perturbations are localized on the periphery.

instead propagate to the inner boundary of the domain. Since no fluid flow shear is involved ($\kappa = 0$) in both simulations, this phenomenon is purely due to the pinch profile shape.

## IV. EXTENDED-MHD SIMULATIONS

The present gyrokinetic model suffers from the absence of electromagnetic effects that are especially important for long-wavelength modes,[22] and from the limitations on the drift velocity, which should not exceed thermal speed. These issues can be addressed in the extended-MHD model, also implemented in the COGENT code. The MHD model simulates the following equations. The continuity equation reads as follows:

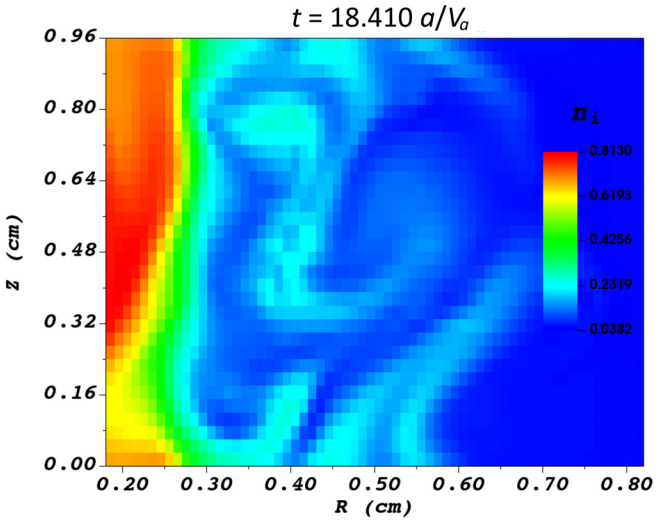


FIG. 9. Gyrokinetic simulations of the $m = 0$, $k_z a = 2.42$ mode for the FuZE-like profile. Normalized ion gyrokinetic density distribution is shown during the nonlinear stage of evolution. The perturbations are spread into the interior of the pinch.

$$\frac{\partial \rho}{\partial t} + \nabla \cdot \mathbf{m} = 0, \tag{16}$$

where $\rho \approx m_i n_i$ is the fluid density and $\mathbf{m} = \rho \mathbf{u}$ is the momentum density with $\mathbf{u} \approx \mathbf{v}_i$ as the electron–ion mass ratio is very small. The momentum density is governed by the MHD equation of motion

$$\frac{\partial \mathbf{m}}{\partial t} + \nabla \cdot (\mathbf{m}\mathbf{u} + \mathbf{I}P + \boldsymbol{\pi}) = \frac{\mathbf{J} \times \mathbf{B}}{c}. \tag{17}$$

Here, $\boldsymbol{\pi}$ is the gyro-viscous pressure tensor, based on Braginskii's formulation. The ion and electron energy densities are defined as

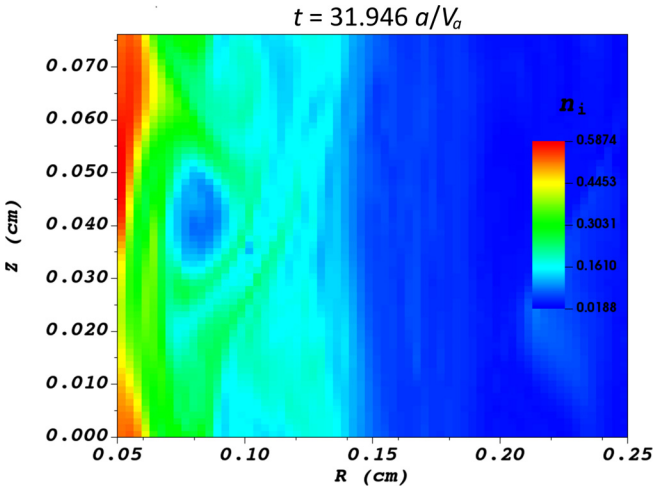


FIG. 10. Gyrokinetic simulations of the $m = 0$, $k_z a = 7.5$ mode for the Bennett profile. Normalized ion gyrokinetic density distribution is shown during the nonlinear stage of evolution. The perturbations are spread into the interior of the pinch.

$$\begin{aligned} \varepsilon_i &= \frac{1}{2}\rho u^2 + \frac{P_i}{\gamma - 1}, \\ \varepsilon_e &= \frac{P_e}{\gamma - 1}. \end{aligned} \tag{18}$$

The equations for $\varepsilon_i$ and $\varepsilon_e$ include diamagnetic heat fluxes $\mathbf{q}_i$ and $\mathbf{q}_e$,

$$\frac{\partial \varepsilon_i}{\partial t} + \nabla \cdot \left[\mathbf{u}(\varepsilon_i + P_i) + \mathbf{u}\boldsymbol{\pi} + \mathbf{q}_i\right] = qn\mathbf{u} \cdot \mathbf{E} + Q_{ie}, \tag{19}$$

$$\frac{\partial \varepsilon_e}{\partial t} + \nabla \cdot \left[\mathbf{u}_e(\varepsilon_e + P_e) + \mathbf{q}_e\right] = -qn\mathbf{u}_e \cdot \mathbf{E} - Q_{ie}. \tag{20}$$

In Eqs. (19) and (20), $Q_{ie}$ is the ion–electron heat exchange, and $\mathbf{u}_e$ is the electron velocity, which is given by

$$\mathbf{u}_e = \mathbf{u} - \frac{\mathbf{J}}{qn}. \tag{21}$$

Equations (16)–(21) are coupled with the generalized Ohm's law,

$$m_e \frac{\partial \mathbf{J}}{\partial t} = q^2 n \left[\mathbf{E} + \frac{\mathbf{u} \times \mathbf{B}}{c} - \frac{1}{qn}\left(\frac{\mathbf{J} \times \mathbf{B}}{c} - \nabla P_e\right)\right]. \tag{22}$$

Ampère's law

$$\frac{\partial \mathbf{E}}{\partial t} = c\nabla \times \mathbf{B} - 4\pi \mathbf{J}, \tag{23}$$

and Faraday's laws

$$\frac{\partial \mathbf{B}}{\partial t} + c\nabla \times \mathbf{E} = 0. \tag{24}$$

The diamagnetic heat flux terms $\mathbf{q}_{i,e}$ are responsible for the existence of certain drift modes in the MHD model, such as the entropy mode studied by different authors.[5,7–9] The model equations are identical to those used in the work of Angus *et al.*[9] with the exception that gyro-viscosity is included here in this work. More details of the model and MHD simulations can be found in Ref. 9.

The extended-MHD model is tested and compared to the electrostatic gyrokinetic one for the FuZE-like pinch profile. The growth rate of a linear $m = 0$ mode is found for different values of the normalized axial wave vector $k_z a$, and the results are shown in Fig. 11. The growth

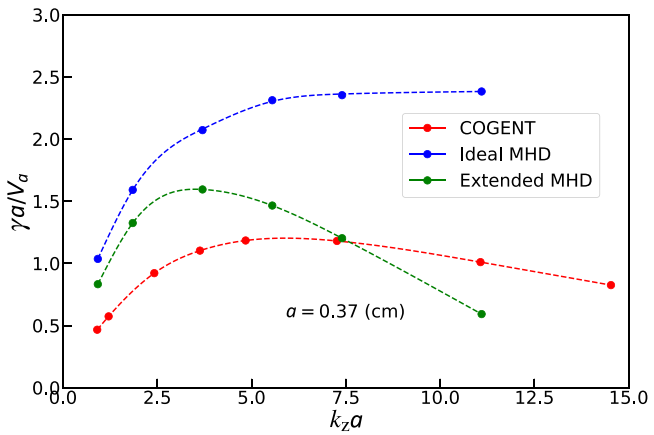


FIG. 11. Comparison of shear-less normalized growth rate curves. Red: gyrokinetic COGENT, blue: ideal MHD, green: extended MHD.

rate roll-over effect at the high-$k$ part of the spectra is reproduced, and it is in a reasonable match with the one from the gyrokinetic simulations.[22] This effect appears in the MHD model due to the gyro-viscous pressure tensor $\boldsymbol{\pi}$. Interestingly, the growth rate obtained by the ideal-MHD simulations is considerably greater than one from the extended-MHD, which suggests that FLR effects play an important role in the linear mode stabilization. Furthermore, this circumstance demonstrates the significance of the pinch profile, as the difference between the ideal-MHD, gyrokinetic, and fully kinetic simulations are much less for the Bennett profile (Fig. 3 from the work of Geyko *et al.*[22]).

The nonlinear mechanism of the stabilization is also verified via the extended-MHD simulations. The wavelengths of the modes are chosen differently, yet they are of the same order that are used in the gyrokinetic simulations, namely, $k_z a = 11.1$ for the short-wavelength and $k_z a = 3.7$ for the long-wavelength mode. The results of the MHD simulations are consistent with the gyrokinetic ones: short-wavelength perturbations nonlinearly saturate on the periphery, while long-wavelength perturbations penetrate into the interior and completely disrupt the pinch.

As it is demonstrated in Fig. 11, the gyrokinetic and extended-MHD models provide quantitatively different results for the linear mode growth rate. The discrepancies between the models also take place when the nonlinear evolution is considered. For example, the mode with $k_z a = 7.26$, which is nonlinearly stable in the gyrokinetic model, is unstable in the extended-MHD model, thus, different value of the mode wavelength was chosen to demonstrate nonlinear stability. Similarly to Fig. 8, two snapshots of nonlinear evolution of the mode with $k_z a = 11.1$ are demonstrated in Fig. 12. The simulation domain in the extended-MHD model is different and captures the axis of the pinch, but the plot is drawn in the same domain as for the gyrokinetic simulations. Figure 12(a) shows the transition from the linear to nonlinear stages where the maximum disturbance of the pinch is observed; Fig. 12(b) shows late time nonlinear evolution. In both cases, the pinch is nonlinearly stable.

Finally, large fluid flow shears $\kappa = \pm 1.1$ are tested, where the variation of the flow over the pinch radius is greater than the Alfvén speed. Even this unrealistic flow shear is shown to be insufficient to fully mitigate linear modes. Figure 13 is a logarithmic plot of the perturbation amplitude of $k_z a = 3.7$ mode as a function of time. The mode is unstable for all three values of $\kappa$, and the only difference is the growth rate, which is nearly unchanged for $\kappa = -1.1$ and noticeably lower for $\kappa = 1.1$. This observation is consistent with the previously mentioned conclusion that, in the case of FuZE-like profile, the amount of shear required for suppression of linear instabilities should be at least comparable to the amount of embedded guiding center drift shear. For the parameters of the problem, it is approximately $\kappa = 1.5$ (see Fig. 6). This requirement is only necessary but not sufficient, which was demonstrated in the simulations.

## V. PROFILE FLATTENING STABILIZATION

As it was shown in Sec. III, nonlinear pinch stabilization can be achieved for short wavelengths, and the stabilization mechanism is the pinch profile itself rather than fluid shear flow. In this section, the nonlinear stabilization is investigated in more detail by varying temperature and density profiles, while maintaining them 'close' to the experimental data. For example, one can argue that experimental data vary depending on the axial location of the measurements and is

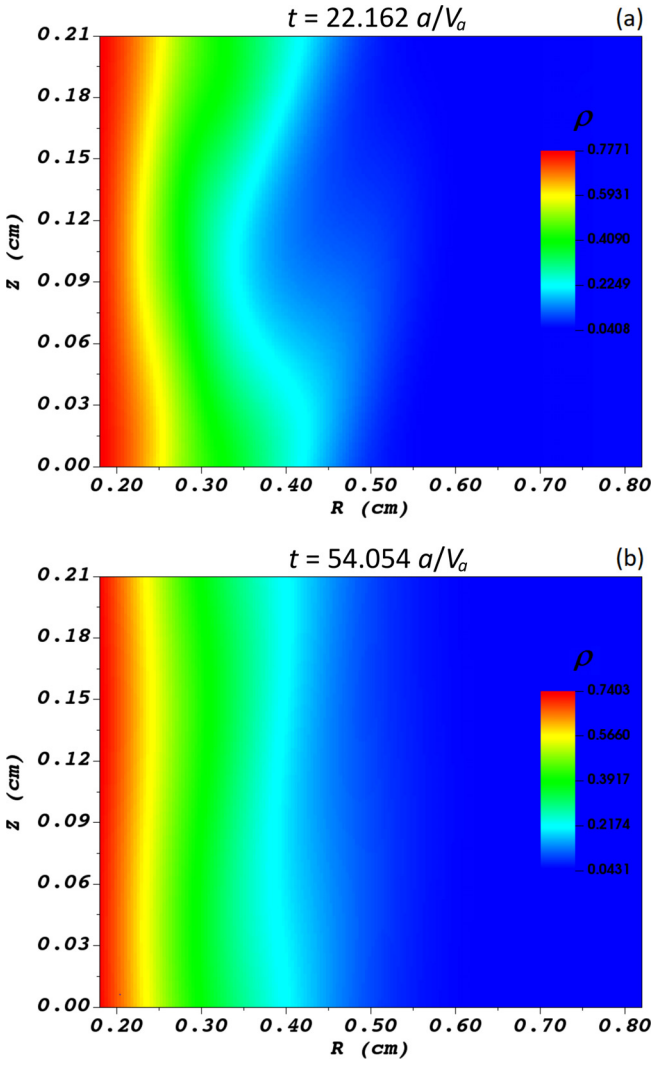


**FIG. 12.** Extended-MHD simulations of the $m = 0$, $k_z a = 11.1$ mode for the FuZE-like profile. Plots demonstrate normalized mass density distribution. Plot (a) shows the transition from the linear to nonlinear stages, where the amplitude of the perturbations is at maximum. Plot (b) shows the nonlinear evolution at later time, where perturbations are localized on the periphery.

obtained with some errors.[13] As a result, fitted analytical profiles are defined with some ambiguity, which can possibly have an impact on stability properties of the pinch. Out of density and temperature profiles, the latter is worse-defined, as the fitting curve does not capture data points even when experimental errors are taken into account (see Fig. 2). A set of gyrokinetic simulations is performed in order to investigate the importance of the temperature profile. To that end, three profiles with FuZE density and constant temperatures are considered: $T_0 = 0.5$, $T_0 = 1.0$, and $T_0 = 2.0$ keV. Since pinch characteristic radius is defined as a point where the magnetic field reaches its maximum, the new profiles have slightly larger scale $a = 0.415$ cm. Thermal and Alfvén velocities, and therefore growth rate normalization, change by a factor $\{\sqrt{1/2};\ 1.0;\ \sqrt{2}\}$, respectively. Figure 14 demonstrates

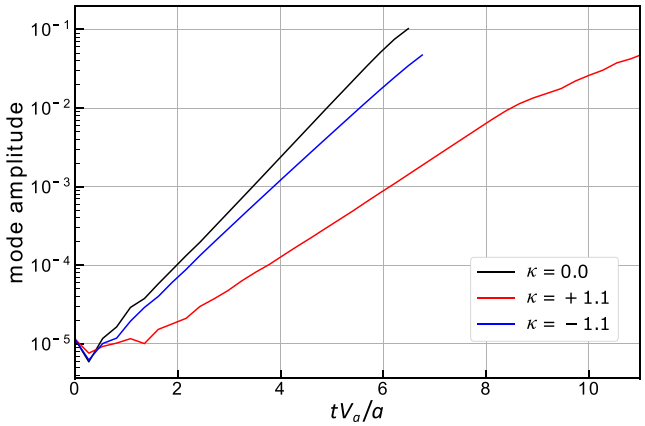


**FIG. 13.** Logarithmic plot of the amplitude of a linear mode with $k_z a = 3.7$ as a function of time for three values of the shear parameter $\kappa$: −1.1, 0.0, and 1.1. In all three cases, the mode is unstable.

comparison of the normalized linear mode growth rate curves for all three constant temperature profiles and a shearless FuZE profile. As expected, the difference of the growth rates for the first three profiles is negligible, because the dynamics is determined by the plasma magnetization $\epsilon = V_{ti}/(a\omega_{ci})$ that is independent of temperature for fixed density, as $B_0^2 = 4\pi n_0 T_0$ from the normalization. However, the difference of the growth rate between FuZE and constant temperature profiles is also relatively small. The shape and the amplitude of the curves are very similar and the main discrepancy is due to scale normalization ($a = 0.415$ cm instead of $a = 0.37$ cm). The similarity also persists when linear mode structure and nonlinear pinch evolution are considered. These simulations demonstrate that the spatial variation of the temperature in the FuZE experiment does not play an important role in stability properties of the pinch.

To study stabilizing role of the density profile, consider the following family of fitting profiles:

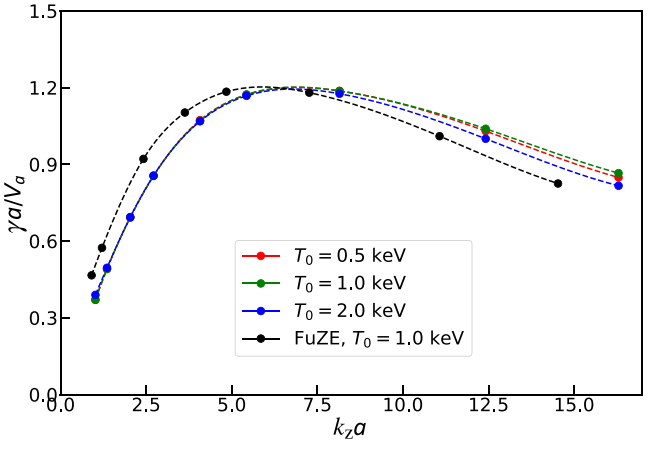


**FIG. 14.** Normalized growth rate of the linear $m = 0$ mode for the shearless ($\kappa = 0$) FuZE-like profile (black) and three profiles with constant temperature (red, green, blue) as a function of the normalized axial wave vector $k_z a$.

$$n(r,p) = 0.05 + 0.855 \cdot p + 0.855 \cdot (1-p) \cdot \exp\left(-\frac{r^2}{0.32} - \frac{r^4}{(0.0177+p)}\right), \quad (25)$$

where $p$ is a *flattening parameter*. The dependence of the density curve on $p$ is shown in Fig. 15. The temperature is kept constant and equal to $T = 1.0$ keV for simplicity, since proven to be unimportant. As $p$ increases, the match between the experimental data and the fitting curve becomes worse, so there is no point to consider $p > 0.04$ if the experimental profile is implied. While the model is indeed inaccurate and should not be considered as a rigorous analysis, it is illustrative and suitable for better understanding of the stabilization phenomena.

Simulations for different values of the parameter $p$ and different wavelengths have been performed. The first observation is that linear mode stabilization cannot be achieved via profile flattening. The growth rate decreases as $p$ gets larger, yet even for $p = 0.04$, which is very far from the experimental data, the normalized growth rate of the most unstable mode ($\lambda = 0.32$ cm) only decreases from 1.05 to 0.6.

The nonlinear behavior is, however, significantly different. The nonlinear perturbation shifts from the interior of the pinch to the periphery, very similar to as it was observed for short-wavelength modes for the FuZE-like pinch in Fig. 8. A density plot of the nonlinear evolution of $\lambda = 1.28$ cm mode is demonstrated in Fig. 16. This mode is shown completely unstable in both gyrokinetic and extended-MHD simulation. For the test profile with $p = 0.04$, all of the perturbations are located at $r > 0.4$, which is at the outer periphery of the pinch. Thus, the interior remains unperturbed and global pinch stabilization can be claimed.

The flattening of the profile basically pushes the instabilities to the periphery and exploits the nonlinear stabilization mechanism described for the short-wavelength modes. Nevertheless, it remains arguable how robust this mechanism can be as the required modifications to the profiles can be so large that they might not adequately represent the experimental data.

## VI. DISCUSSION AND CONCLUSION

The stability properties of $m = 0$ modes in a FuZE-like type of a Z-pinch have been studied in the present work. The pinch profile is

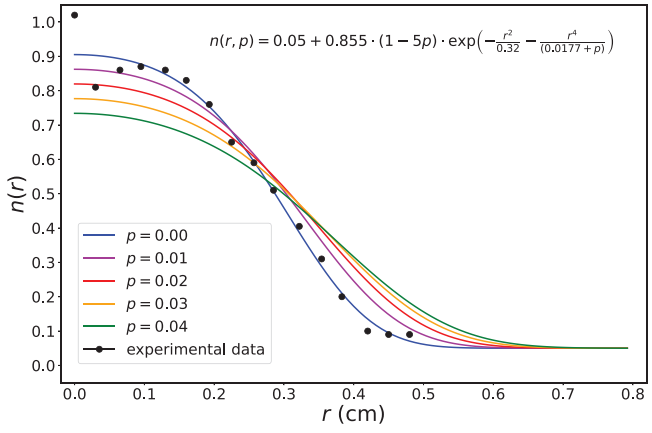


**FIG. 15.** Possible relaxation of the density profile fitting curve for five different values of the flattening parameter $p$ in Eq. (25).

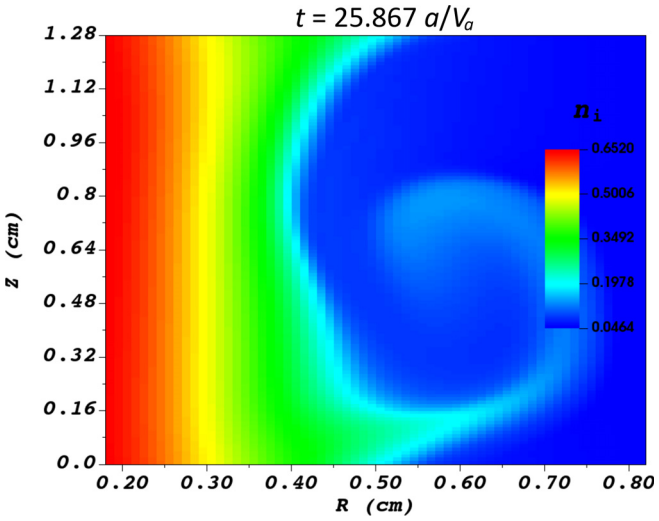


**FIG. 16.** Gyrokinetic simulations of the $m = 0$, $k_z a = 1.815$ mode for the *relaxed* FuZE-like profile with $p = 0.04$. Normalized ion gyrokinetic density distribution is shown during the nonlinear stage of evolution. The perturbations are saturated on the periphery.

shown to play an important role in both the growth rate of linear modes and stabilization possibilities via axially sheared fluid flow. The key difference of any realistic profile, including the FuZE-like one, from the model Bennett profile is that the particle guiding center velocity has an intrinsic embedded shear, even for a zero fluid flow. Unlike the Bennett case, the presence of a fluid flow shear does not necessarily lead to the mode mitigation and the reduction of the growth rate, but can also make the system even more unstable. The intrinsic guiding center flow, however, for the parameters of the FuZE experiment, has quite a pronounced (up to Alfvén speed over the pinch radius) local shear; thus, no moderate (sub-Alfvénic) flow shear is sufficient to change the instability behavior drastically.

These conjectures have been confirmed by numerical simulations performed with the COGENT code. Both electrostatic gyrokinetic and extended-MHD models agreed that the growth rate of the linear $m = 0$ mode is not considerably affected by a subthermal fluid shear flow. The changes of the growth rate corresponding to the sign of the applied shear found to be consistent with the guiding center drift picture. The nonlinear stabilization of the short-wavelength modes ($ka \geq 7.5$ in gyrokinetic, $ka \geq 11.1$ in extended-MHD simulations) has been observed. The mechanism of such stabilization is due to nonlinear saturation of the modes on the pinch periphery such that the interior of the pinch remains unperturbed. The global pinch stability has not been achieved, as the mechanism is unable to stabilize long-wavelength modes.

The results presented in this work do not support the conjecture that Z-pinch stabilization observed in some experiments is due to a sheared axial flow of the plasma. It is shown that if a realistic pinch profile is considered, no sub-Alfvénic fluid flow shear is sufficient for stabilization of linear modes. Relaxation of pressure gradients, described in Sec. V, is not sufficient either. A possible explanation is that the linear modes are always unstable and the global pinch stability is achieved by a combination of nonlinear saturation of the modes and finite Larmor radius effects. In order to proceed and investigate this phenomenon thoroughly, more detailed computational models are needed. To that end, higher order FLR effects are developed, included and being tested in the COGENT code, as well as further improvements of the extended-MHD model are being done.

The failure of the present model to adequately describe experimental observations might be also due to misinterpretation of experimental data. For example, a commonly accepted assumption of a stationary axisymmetric pinch might be invalid, since not realized in experiments. In this case, a large series of experiments has to be performed in order to verify a proper setup for analytical models. This is a subject of future research and out of scope of the present work.

## ACKNOWLEDGMENTS

This work was performed under the auspices of U.S. DOE by LLNL under Contract No. DE-AC52–07NA27344 and was supported by LLNL-LDRD under Project No. 18-ERD-007.

## DATA AVAILABILITY

The data that support the findings of this study are available from the corresponding author upon reasonable request.

## REFERENCES

[1]P. Reynolds and J. D. Craggs, Philos. Mag. **43**, 258 (1952).
[2]I. V. Kurchatov, J. Nucl. Energy **4**, 193 (1957).
[3]P. Freidberg, *Ideal Magnetohydrodynamics* (Plenum, New York, 1987).
[4]R. Carruthers and P. A. Davenport, Proc. Phys. Soc., London, Sect. B **70**, 49 (1957).
[5]B. B. Kadomtsev, J. Exp. Theor. Phys. **10**, 780 (1960); available at http://www.jetp.ac.ru/cgi-bin/e/index/e/10/4/p780?a=list.
[6]P. Ricci, B. N. Rogers, W. Dorland, and M. Barnes, Phys. Plasmas **13**, 062102 (2006).
[7]P. Ricci, B. N. Rogers, and W. Dorland, Phys. Rev. Lett. **97**, 245001 (2006).
[8]A. N. Simakov, P. J. Catto, and R. J. Hastie, Phys. Plasmas **8**, 4414 (2001).
[9]J. R. Angus, M. Dorf, and V. I. Geyko, Phys. Plasmas **26**, 072505 (2019).
[10]U. Shumlak, R. P. Golingo, B. A. Nelson, and D. J. D. Hartog, Phys. Rev. Lett. **87**, 205005 (2001).
[11]U. Shumlak, B. A. Nelson, R. P. Golingo, S. L. Jackson, E. A. Crawford, and D. J. D. Hartog, Phys. Plasmas **10**, 1683 (2003).
[12]U. Shumlak, B. A. Nelson, E. L. Claveau, E. G. Forbes, R. P. Golingo, M. C. Hughes, R. J. Oberto, M. P. Ross, and T. R. Weber, Phys. Plasmas **24**, 055702 (2017).
[13]Y. Zhang, U. Shumlak, B. A. Nelson, R. P. Golingo, T. R. W. A. D. Stepanov, E. L. Claveau, E. G. Forbes, Z. T. Draper, J. M. Mitrani, H. S. McLean, K. K. Tummel, D. P. Higginson, and C. M. Cooper, Phys. Rev. Lett. **122**, 135001 (2019).
[14]U. Shumlak, J. Appl. Phys. **127**, 200901 (2020).
[15]A. D. Stepanov, U. Shumlak, H. S. McLean, B. A. Nelson, E. L. Claveau, E. G. Forbes, T. R. Weber, and Y. Zhang, Phys. Plasmas **27**, 112503 (2020).
[16]R. P. Golingo, U. Shumlak, and B. A. Nelson, Phys. Plasmas **12**, 062505 (2005).
[17]U. Shumlak, C. S. Adams, J. M. Blakely, B. J. Chan, R. P. Golingo, S. D. Knecht, B. A. Nelson, R. J. Oberto, M. R. Sybouts, and G. Vogman, Nucl. Fusion **49**, 075039 (2009).
[18]U. Shumlak and C. W. Hartman, Phys. Rev. Lett. **75**, 3285 (1995).
[19]T. D. Arber and D. F. Howell, Phys. Plasmas **3**, 554 (1996).
[20]J. R. Angus, J. J. Van De Wetering, M. A. Dorf, and V. I. Geyko, Phys. Plasmas **27**, 122108 (2020).
[21]I. Paraschiv, B. S. Bauer, I. R. Lindemuth, and V. Makhin, Phys. Plasmas **17**, 072107 (2010).

[22]V. I. Geyko, M. Dorf, and J. R. Angus, Phys. Plasmas **26**, 062114 (2019).
[23]K. Tummel, D. P. Higginson, A. J. Link, A. E. W. Schmidt, H. S. McLean, D. T. Offermann, D. R. Welch, R. E. Clark, U. Shumlak, B. A. Nelson, and R. P. Golingo, Phys. Plasmas **26**, 062506 (2019).
[24]T. D. Arber, M. Coppins, and J. Scheffel, Phys. Rev. Lett. **72**, 2399 (1994).
[25]W. H. Bennett, Phys. Rev. **45**, 890 (1934).
[26]W. H. Bennett, Phys. Rev. **98**, 1584 (1955).
[27]M. A. Dorf, R. H. Cohen, M. Dorr, T. Rognlien, J. Hittinger, J. Compton, P. Colella, D. Martin, and P. McCorquodale, Phys. Plasmas **20**, 012513 (2013).
[28]G. F. Chew, M. L. Goldberger, and F. E. Low, Proc. R. Soc. **A 236**, 112 (1956).
[29]P. Bellan, *Fundamentals of Plasma Physics* (Cambridge University Press, 2006).